

IMAGER FOR MAST

A narrow band imager proposal for Multi Application Solar Telescope
Prepared by Shibu K. Mathew, Udaipur Solar Observatory, India

Abstract

This report details a proposal for narrow band imager for the Multi Application Solar Telescope (MAST) to be installed at Udaipur Solar Observatory (USO) in the beginning of 2009. The heart of the system is two Fabry-Perot etalons working in tandem. Combining with two interference filters centered at 6173\AA and 8542\AA the etalons will give a spectral resolution of 54 m\AA ($R = 114\text{ k}$) and 104 m\AA ($R = 82\text{ k}$) at the above wavelengths, respectively. The substrate of the etalons is made of Lithium Niobate electro-optic crystal. The refractive index of the crystal can be changed by applying voltage, and this property is used in tuning the filter. In this report we present the complete description of a narrow band imager, which could provide near simultaneous spectral observations in two solar absorption lines formed at two different heights (photospheric - FeI 6173\AA and chromospheric - CaII 8542\AA line) in the solar atmosphere.

1. Introduction

MAST is a project for installing a modern solar telescope with adaptive-optics capabilities for image stabilization and seeing corrections. The telescope is an off-axis 50 cm reflector which provides a full field-of-view of 6arc-min. A spatial resolution of 0.5arc-sec could be achieved with this telescope using the adaptive optics system for a limited field-of-view of ~ 15 arc-sec. The salient features of the telescope are listed in table 1.

Table 1. *Characteristics of the main telescope*

Primary mirror clear aperture	50 cm, off-axis
Max available field-of-view (FOV)	6 arc-min
Output wave-front error	$\lambda/10$ rms over FOV
Achievable resolution with adaptive optics installed	0.5arc-sec (for 15arc-sec)

More details on the telescope can be found in the MAST web page <http://www.prl.res.in/~uso/mast/mast.html>. The telescope will be feeding light to two back-end instruments, a narrow-band filter based imager and a spectrograph. A polarimeter is also planned for the polarization measurements, which will be introduced ahead of the above instruments. In this report, the proposed narrow-band imager for the MAST telescope is discussed.

2. Science goals

Understanding the solar magnetic and velocity fields in small and large scale solar structures and active regions are the main science goals for the narrow band imager. A list of major science goals of the MAST instrument can be found in the telescope proposal. Operating in conjunction with a Stokes polarimeter, we plan to specifically address the following problems using the narrow band imager:

- The topology and evolution of emerging magnetic flux regions leading to the solar activities such as flares and coronal mass ejections
- Magnetic and velocity structure of sunspots and small scale features such as pores in photosphere and chromosphere.
- Decay of sunspots and their relation to moving magnetic features
- Quantification of helicity in solar active regions and their relation to explosive events
- Dynamics in small scale structures such as granules and inter-granular lanes

By measuring the vector magnetic and velocity fields with good temporal and spatial resolution, most of the above science goals can be realized.

3. Fabry-Perot etalons as narrow band filters

Recently, Fabry-Perot (FP) etalons are widely used as narrow band filters in solar observations.^[1,2,3] Compared to the conventionally used bi-refringent Lyot filters the FP etalons have added advantages of fast tunability and higher throughput. Also, by using different blocking filters it is possible to tune the filter to different wavelength bands which is useful for near-simultaneous multi-wavelength observations. There are etalons which differ in their mode of operation. The easily tunable etalons are piezo-electrically adjusted variable air-spaced and electro-optically adjusted variable refractive index etalons. Later, we compare the above two types of etalons for their advantages and disadvantages.

Before comparing different types of etalons, we discuss the basic equations governing the properties of the etalons. The transmitted intensity through the etalon is described by the Airy formula,

$$I_t = I_i [1 + F \sin^2(\delta/2)]^{-1}$$

where, I_t the transmitted intensity, I_i the incident intensity, F the reflectivity finesse, and δ the phase. The *reflectivity finesse* F is defined as $4R/(1-R^2)$ where R is the reflectivity of the coated surfaces. The phase shift $\delta = 4\pi\mu d \cos\theta / \lambda$, where μ is the refractive index of the medium, d is the spacing, θ the angle of incidence with in the medium, and λ the wavelength. The transmission is periodic, and the maxima (channels)

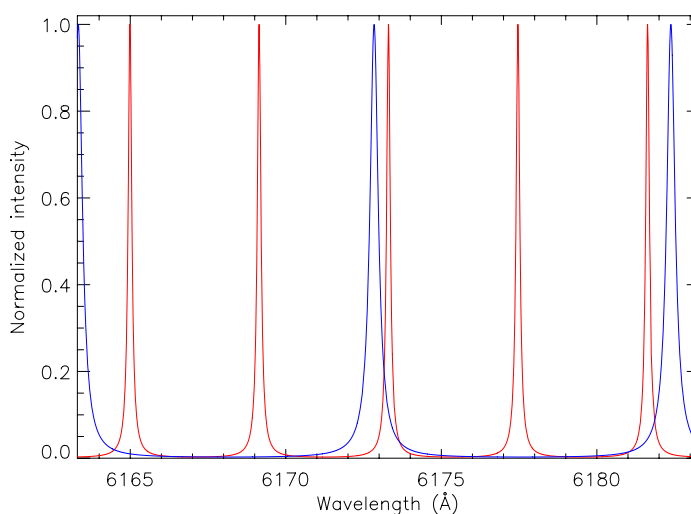


Fig. 1. Channel spectra for an air-spaced (blue) and a lithium niobate (red) etalons with same spacing/thickness and the same reflectivity (90%). The reduced FSR for the case of Lithium Niobate etalon is due to the increase in effective optical thickness of the crystal which is a product of the refractive index and the physical thickness of the crystal.

are at wavelengths $\lambda = 2\mu d \cos\theta / m$, where m is the order, an integer. The free spectral range $FSR = \lambda^2 / 2\mu d \cos\theta$ is the wavelength spacing between the two successive

maxima. The full width at half-maximum of the transmitted channel is given by $\Delta\lambda = FSR/N_r$, where N_r is the *finesse* and is given by $\pi\sqrt{R}/(1-R)$ or $\lambda^2/\pi\mu d\sqrt{F}$ in terms of F . Figure 1 shows the spectral channels for an air-spaced (blue, $\mu = 1$) and a lithium niobate (red, $\mu = 2.29$) etalons with same spacing/thickness around 617 nm for a reflectivity of 90%. The difference in FSR and the FWHM in these two cases are due to the difference in refractive index of the medium (and thus the resulting optical path). A large value of FSR is desirable in narrow band filter design, but for the same reflectivity decreasing the spacing will also increase the FWHM of the band-pass.

The piezo-electrically tuneable etalons are constructed using two parallel glass plates, the medium between the plate is air ($\mu = 1$). One of the plates is mounted on piezo stacks, and thus could be moved by applying voltage on these stacks. This changes the spacing between the plates and thus tunes the pass band. The parallelism between the plates is maintained by a capacitance servo loop. In electrically tuneable solid state etalons, the medium is an opto-electric material, e.g, Lithium Niobate is an opto-electric material and is usually used for this purpose. Thin wafer of this crystal is polished and reflective coatings are applied on both the faces. Transparent Indium- Tin Oxide coating is also applied to the faces, which acts like electrodes. Application of voltage across the crystal changes the refractive index of the crystal and this property is used for tuning the pass-band.

Both the piezo-electrically tuneable etalons and electrically tuneable Lithium-Niobate etalons have their own advantages and disadvantages. Availability of high finesse etalons with large size is one of the advantages of piezo-electrically tuneable etalons. Effective finesse of 40 and above and sizes of up to 100mm is available with piezo-electrically tuneable etalons. In the case of Lithium Niobate etalons complex process of polishing the thin wafer makes it difficult to produce the etalons above an effective finesse of 30. The high refractive index of the Lithium Niobate crystal (~ 2.3) amplifies any surface irregularities, and for the same fabrication finesse the crystal should be polished to more than four times the surface accuracy of the glass substrates used in the air-spaced etalons. But once the surface is polished, the parallelism between the surfaces is maintained, which avoid the need of any complex electronics used as in the air-spaced etalons. This makes the Lithium-Niobate etalons easy to use.

Another important factor is the wavelength shift and the widening of the pass band when the etalon is used in collimated and telecentric beams, respectively. The wave length shift of the transmission peak due to the incidence angle is inversely proportional to the square of the refractive index of the medium, and is given by $\delta\lambda = -(\lambda/2)(\theta/\mu)^2$. The Langrange optical invariant, which is the product of the beam aperture and the angle of the chief ray, can be used to determine the maximum angle of incidence in the filter

* Even though MAST telescope can provide a maximum of 6arc-min FOV, initially we will allow only 3 arc-min through the narrow-band imager, which is adequate enough to cover a typical active region. Later on, a different set of additional lenses will also be used for reducing the f-number and thus to allow 6 arc-min FOV through the etalons. This configuration will in-effect widens the pass-band and thus reduces the spectral resolution. By interchanging the lens system we will be able to obtain both 3 arc-sec and 6 arc-min FOV observations, but later with a lower spectral and spatial resolution.

system and is given by $\theta = \frac{1}{2} FOV(A_{tele} / A_{fp})$, and thus can be used to analyse the effect of angle of incidence on the filter passband. This relation is valid for both collimated and telecentric beams^[4]. For a 50mm filter aperture and 3arc-min field-of-view* in MAST (0.5 m aperture) the maximum angle of incidence is around 15arc-min. Now, in the collimated setup every point in the image plane corresponds to incident rays with specific angle of incidence^[3]. The angle of incidence increases towards the edge of the field-of-view and this produces a blue shift in the transmitted wavelength. In case of an air-spaced etalon this wavelength shift towards the edge of the 3arc-min field-of-view at 6173Å is around 59mÅ. Due to the higher refractive index of the medium, in the case of Lithium Niobate etalon, the wavelength shift for the same field-of-view is only 11mÅ. In Fig. 2 we display the wavelength shift in the transmitted light across the 3 arc-min field-of-view for an air-spaced and Lithium Niobate etalons.

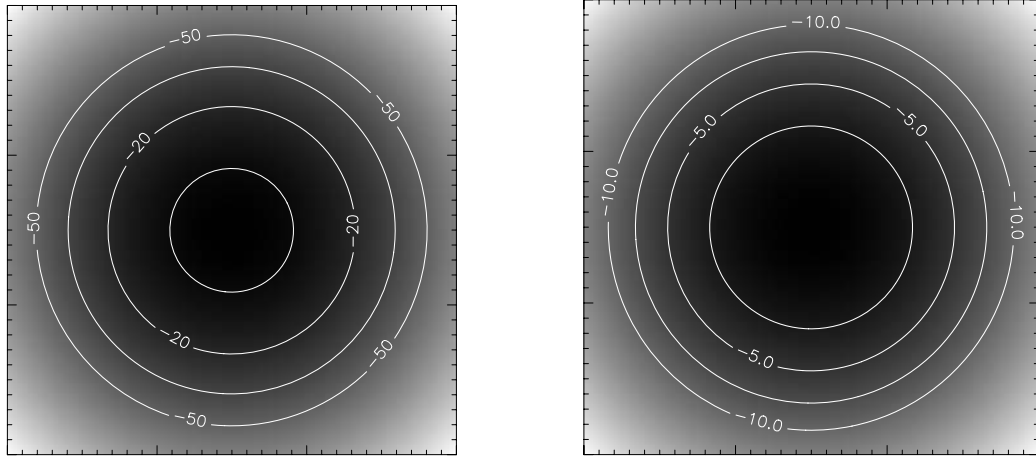


Fig. 2. Air-spaced (left) and Lithium Niobate (right) Fabry-Perot etalons in collimated set-up. The contours show the wavelength shift in mÅ for a circular field-of-view of 3 arc-min for the same size (50 mm) Fabry-Perot etalons. The shift in wavelength in the case of LiNbO₃ etalon is much smaller than that in the air-spaced etalon.

In telecentric set-up the beams which form each point in the image across the field-of-view have the same cone angle and the maximum ray angle corresponds to maximum angle of incidence given by the Langrange invariant. In effect, this cone angle produces a broadening of the effective pass band which is given by $FWHM_{eff} = [FWHM^2 + \delta\lambda^2]^{1/2}$ and is same for all points in the image plane. Assuming a 54mÅ pass-band for the etalon and for 3 arc-min field-of-view, the effective pass band will be around 79mÅ and 55mÅ for the air-spaced and Lithium Niobate etalons, respectively.

From the above discussion we can conclude that, use of Lithium Niobate etalons provide smaller wavelength shifts or broadening of the pass band compared with air-spaced etalons for the same field-of-view observations. In other words, in order to have the same wavelength shift and similar broadening of the filter profile, in comparison to Lithium Niobate etalon a larger aperture air-spaced etalon is required. For example,

limiting the wavelength shift similar to that in the 50mm Lithium Niobate etalon, a 115mm aperture (2.29 times the aperture) air-spaced etalon should be used for 3 arc-min field-of-view observations.

Considering the field-of-view advantage and ease in operation we prefer Lithium Niobate etalons over the air-spaced etalons for our narrow band imager. In table 2 we compare some of the properties of the Lithium Niobate and piezo-electrically tuned air-spaced etalons. Commonwealth Scientific and Industrial Research Organisation (CSIRO), Australia, is the main supplier of Lithium Niobate etalons. There are a few places where Lithium Niobate etalons are currently being used/proposed for solar observations. At Udaipur Solar Observatory (USO), a line-of-sight magnetograph^[2] was operating during 1996-1998, using z-cut Lithium Niobate etalon (160mÅ pass-band at 6122Å) as a narrow band filter. Recently the above magnetograph has been replaced by a newly developed Solar Vector Magnetograph (SVM), in which an air-spaced piezo-electrically tuned etalon from ICOS is used for narrow band imaging^[5]. The Applied Physics Laboratory (APL), Flare Genesis balloon experiment use Lithium Niobate etalons for vector magnetic field measurements^[6]. Regular H α Doppler observations are carried out by Sara F. Martin at Helio Research using a filter developed by y-cut Lithium Niobate etalon. Also, the Imaging Magnetograph eXperiment (IMaX) in Sunrise (balloon experiment to be conducted from Antarctica) will be using a z-cut Lithium Niobate etalon in double pass mode^[7]. Recently, ETH, Zurich group procured two y-cut Lithium Niobate etalons and are being currently used for polarimetric observations^[8] in conjunction with ZIMPOL.

Table 2. Comparison of piezo-electrically tuned air-spaced etalon and Lithium Niobate etalon.

Parameters	Air-spaced, Piezo electric	Lithium Niobate
Parallelism	Adjusted by the piezo stacks, need to check and maintain	Determined by the polishing of the material, remains stable
FOV wavelength variation	Higher ($\delta\lambda = -\lambda\theta^2$)	Lower ($\delta\lambda = -\lambda\theta^2 / \mu^2$)
Size of the etalon for the same field-of-view wavelength variation	Bigger	Smaller by a factor of μ
Tuning voltage	Lower (in the range 0 – 600 Volts)	Higher (in the range of ± 3000 Volts)
Available sizes	Sizes up to 150mm is available (used in ISOON from ICOS)	Sizes up to 60mm is available (from CSIRO)
Effective Finesse	Available up to 50	Available up to 35, normally limited to 25

4. Narrow band Imager for MAST

The objective of the narrow band imager is to obtain ‘wide field’, 2D images and vector magnetic field observations with high temporal and spatial resolutions. We are aiming for a moderate spectral resolution of around $50\text{m}\text{\AA}$. Complimentary high spectral resolution ($\sim 15\text{m}\text{\AA}$) images will be obtained with the proposed spectrograph, which need time for scanning to produce a 2D map with adequate field-of-view. Tuning the narrow band filter profile at few positions across the spectral line, and by analysing polarized images, it would be possible to retrieve the magnetic field information^[9]. For high temporal resolution vector magnetograms, polarized images could be obtained by fixing the filter profile in one of the wings of the spectral line. In the following, we describe the details of the proposed narrow band imager for the MAST.

a) Optical layout of the Imager

The optical layout of the narrow band imager is shown in the figure 3. After considering the small pass-band broadening for 3 arc-min field-of-view and 50mm etalon, we choose a telecentric configuration for our system. Telecentric configuration avoids any field-of-view dependent pass-band shift in transmitted profile, as it should be the case in the collimated setup. Light from the telescope after passing through the polarimeter, adaptive optics system and an appropriate re-imaging lens makes an f-number of 110 image close to the interference blocking filter **IF**. The 3 arc-min field-of-view will results in a 48mm image at the focal plane. This large f-number is required to fill the 50mm Fabry-Perot etalon to its full extent in-order to restrict the broadening of the filter profile due to large angle of incidence. One of the Fabry-Perot (**FP1**) is placed in front of the blocking filter and the second one (**FP2**) after the interference filter. Keeping the blocking filter in between the two Fabry-Perot etalons will considerably reduce the ghost reflections between the two. **L1** is a collimating lens with focal length of 750 mm. A Newport PAC097 is used for this purpose while producing this layout.

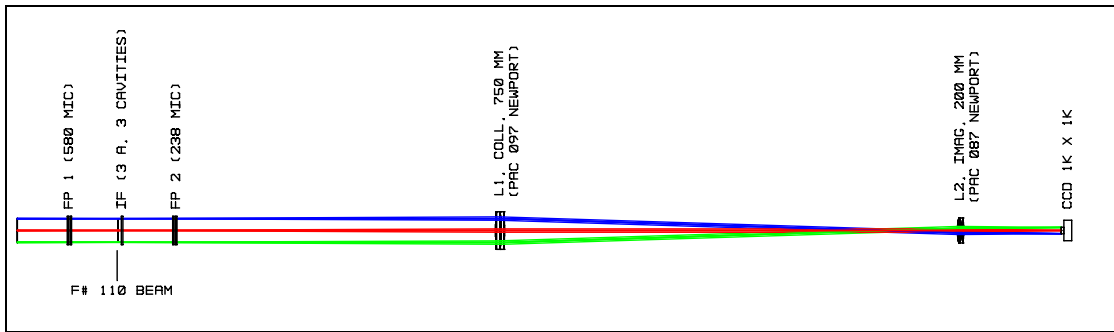


Fig. 3 Optical layout of the narrow-band imager for the MAST telescope. The two Fabry-Perot etalons and interference filters are placed close to the first focal plane. L1 and L2 are the collimator and imaging lens, respectively.

The beam is passed through another lens **L2** (Newport PAC087) for re-imaging. The collimated beam from **L1** makes it easy to choose a re-imaging lens of available size and also give enough freedom in placing the CCD at an appropriate distance. In our case the

imaging lens is placed at around 900mm away from **L1**. **L2** reduces the magnification at the final image plane to 0.266. This will make an image of 12.88mm size for 3 arc-min field-of-view on the CCD chip. This image size is right enough to fill an 1k×1k CCD with 13mm imaging area. The final spatial resolution achieved in the CCD plane is 0.176"/pixel, and is sufficient to image in the diffraction limit of the telescope.

b) Tandem Lithium Niobate Fabry-Perot etalon filter

We intend to use two Lithium Niobate Fabry-Perot etalons and initially two blocking filters to construct a narrow band filter. The filter will operate at two wavelength bands centred at 6173Å and 8542Å. The use of two etalons with different thickness in tandem will increase the free-spectral-range, while maintaining the FWHM of the thickest etalon. The combined transmission profile is the product of the individual etalons and the resultant FWHM is given by $\delta\lambda = \lambda_0^2 / \pi\mu d_0 \sqrt{F(1+k^2)}$, where **k** is the thickness ratio of the two etalons i.e. **d₁/d₀**.

For calculating the optimum thickness and thickness ratio of the etalons we adopted the method described in Kentischer et al.^[3]. The constraints while selecting the Lithium Niobate etalons are the available minimum thickness of the crystal and the maximum finesse. The minimum thickness advised for a safe voltage tuning is around 200 microns. A fabrication finesse of 25 is normally made available by the manufacturer (Australian Centre for Precision Optics, CSIRO, Australia). It should also be noted that in this type of etalons, once fabricated it is impossible to change the thickness and the tuning is carried out mainly by changing the refractive index.

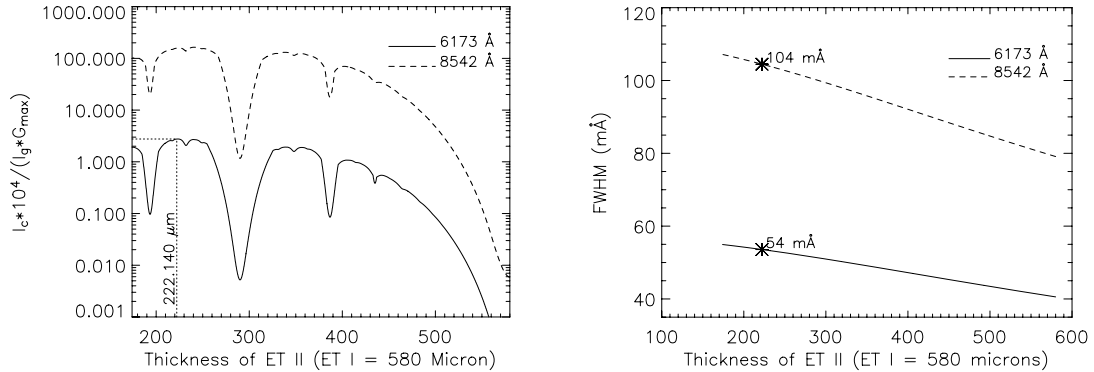


Fig. 4. The performance in terms of signal-to-noise/maximum ghost and FWHM (left) and the resulting FWHM (right) for tandem etalons with different thickness ratios. For the first etalon, a thickness of 580 microns is assumed. A two cavity, 3Å blocking filter is used for the channel selection. The plots are made for 6173 Å and 8542 Å wavelengths.

For the first etalon we used a thickness of 580 microns, which is similar to the optical thickness (1.3 mm, refractive index times the crystal thickness) of the etalon used in TESOS^[3]. A 2-cavity, 3Å interference filter is used as the blocking filter. The SNR (I_c/I_g) is obtained by computing the ratio of integrated intensity of the central peak

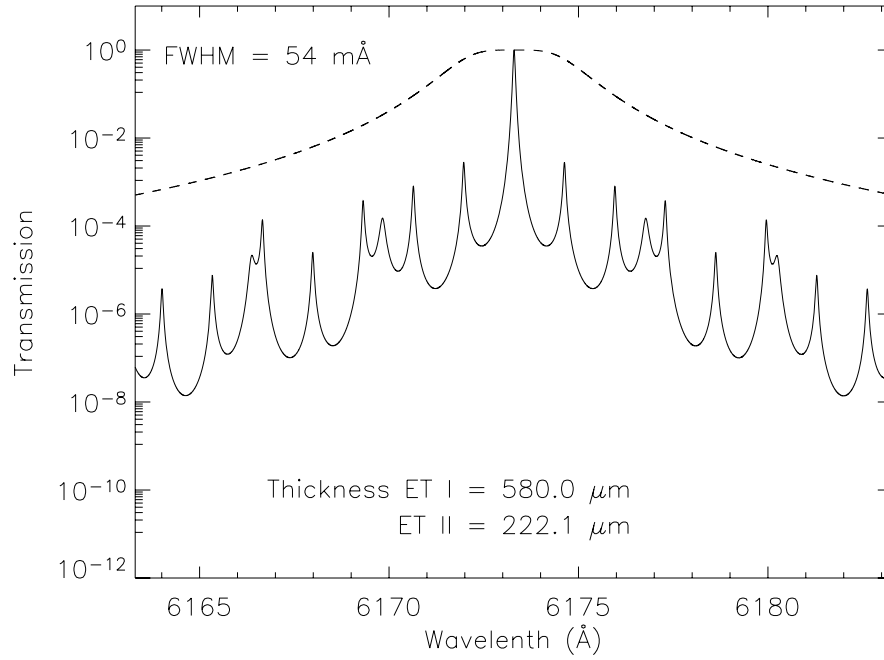


Fig 5. *The resultant filter profile computed from tandem combination of two Lithium Niobate etalons for the wavelength band including 6173Å*

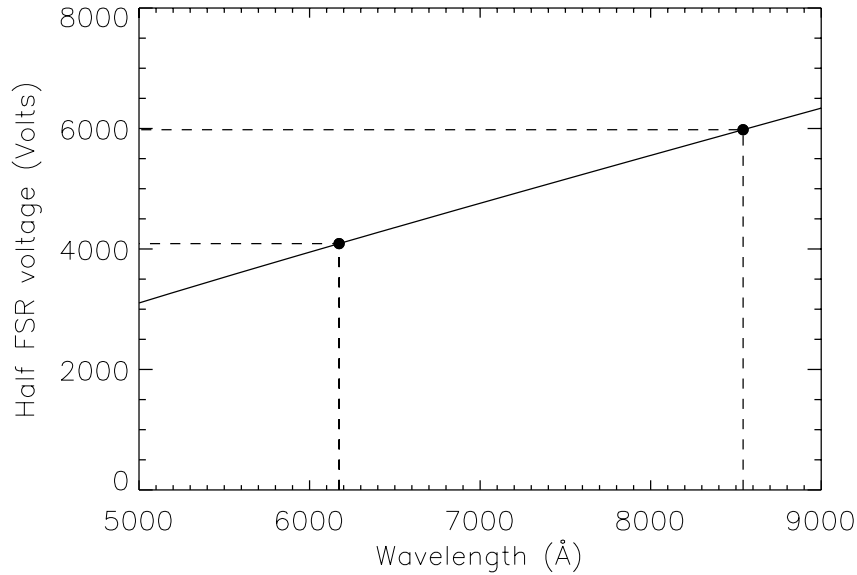


Fig 6. *Half-FSR voltage computed for z-cut Lithium Niobate etalon. The voltage values for the wavelengths which will be used in our observations are marked by dashed lines*

(taking 2 times FWHM in wavelength on either side) to the off-band peaks and the intensity of strongest off-band peak. Right panel in figure 4 shows the result. For a thickness ratio of around 0.382 we obtain the best result for this combination. This gives

a thickness of 222.1 microns for the second etalon and resulting FWHM of 54mÅ at 6173Å. The combined filter profile computed for 6173Å wavelength is shown in figure 5. It should be noted that the profile shown here is for normal incidence and the angle of incidence due to our finite field-of-view will broaden the filter profile to a slightly higher value (for our 3 arc-min field-of-view it will be 55 mÅ). It was found that the nearest off-band peak has an intensity of less than 0.5%. The same spacing ratio can be also be used for imaging at 8542Å, this yields reduced spectral resolution of 104mÅ assuming the same reflectivity finesse for the etalon at this wavelength.

In order to obtain the full profiles of the spectral lines it is required to tune the etalon to various wavelength positions on the absorption line. Tuning of Lithium niobate etalon is carried out by applying voltage across the substrate. This in effect changes the refractive index of the crystal and shifts the transmission peak accordingly. The voltage tuneability In order to obtain the full profiles of the spectral lines it is required to tune the etalon to various wavelength positions on the absorption line. Tuning of Lithium niobate etalon is carried out by applying voltage across the substrate. This in effect changes the refractive index of the crystal and shifts the transmission peak accordingly. The voltage tuneability is normally expressed in $\frac{1}{2}\text{FSR}$ voltage which is a constant for any thickness of the crystal and for a given wavelength. The half-FSR voltage for an z-cut crystal is given by $V_{1/2} = \pm\lambda / 2\mu_0^3 r_{13}$, where μ_0 is the refractive index, λ the operating wavelength, and r_{13} the electro-optic coefficient of the z-cut crystal. Figure 6 shows the computed $\frac{1}{2}\text{FSR}$ voltages for different wavelengths. An experimentally determined value of 6.28 pm/volts

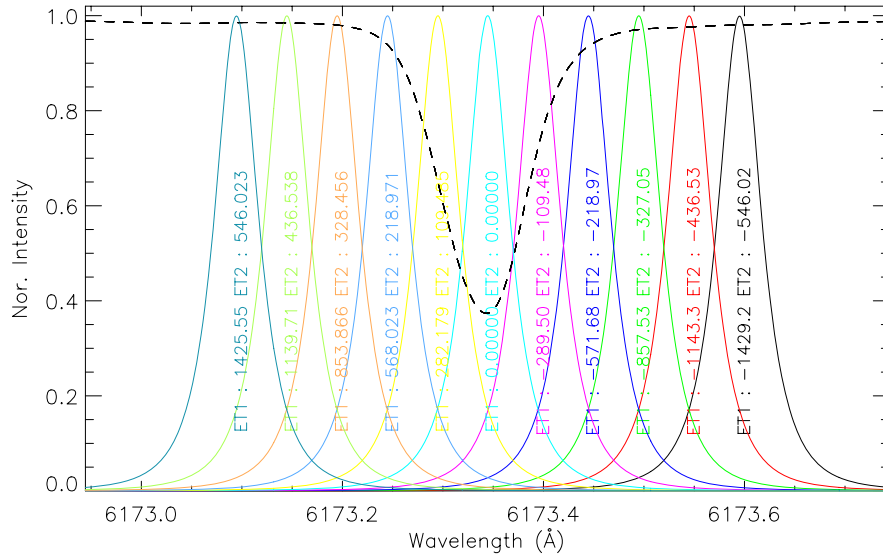


Fig 7. The computed voltages and the location of the resultant filter pass-band along with the FeI 6173.34 Å solar absorption line(dashed line). ET1 and ET2 are 580 and 222.1 microns etalons, respectively.

for r_{13} ^[10] is used in our calculations. The half-FSR values for the first and second etalons at 6173Å are 0.717Å and 1.872Å, respectively. The computed voltages for half-FSR

tuning for the etalon at this wavelength are around ± 2000 Volts (a total of 4000 Volts). For 8542Å the half-FSR voltage is around ± 3000 Volts (a total of 6000 Volts). The above voltages are safe enough to apply across the crystal and thus the etalon can be used for scanning the entire wavelength range. In Fig. 7 we show the tuning voltages required for both the etalons to cover the entire wavelength range in 10mÅ steps, assuming the filter is initially tuned at the centre of the Fe I 6173.34Å line shown with dashed lines in the figure.

c) Detector and data acquisition system

Selection of camera is done taking the following factors into account. The camera should provide a quantum efficiency better than 60% for the wavelength range of 600 – 900 nm. Shutterless operation (frame transfer) is preferred due to the short exposure times employed in our observations. Otherwise, the finite speed of the mechanical shutters normally leaves an impression on the chip during short exposures, which is often difficult to correct while flat-fielding. The frame rate should be large enough to have images with high temporal resolution. Acton PhotonMAX 1024B meets most of these criteria. This camera is installed with 1024×1024 e2v EMCCD chip (electron-multiplying CCD) having square pixels of 13×13 microns and 100% fill factor. The total imaging area is 13.3×13.3mm which is sufficient for our system to image 3 arc-min field-of-view. Quantum efficiency (QE) is better than 60% for 600 – 850 nm wavelength range. Thermo electric cooling makes the dark current as low as 0.04 e⁻/pixel/sec. The camera works in two modes, ‘on-chip multiplication gain amplifier’ with an output noise 730 ke⁻ and a ‘traditional amplifier’ mode with 80 ke⁻ pixel full-well capacity. The camera can deliver 8.5 full frames per second with 16-bits accuracy.

The available PCI interface in the camera can be used for all our image acquisition purposes. A standard Pentium Intel Duo Core Processor PC running on Windows XP/Linux will be used for data acquisition and for synchronising various other activities with the image acquisition.

d) Enclosure

All the optical components and the camera will be placed in an enclosure to avoid any scattered light and other contaminants. Assuming an air-conditioned environment of 22±3°C in the observing room, we intend to keep the enclosure at around 25°C.

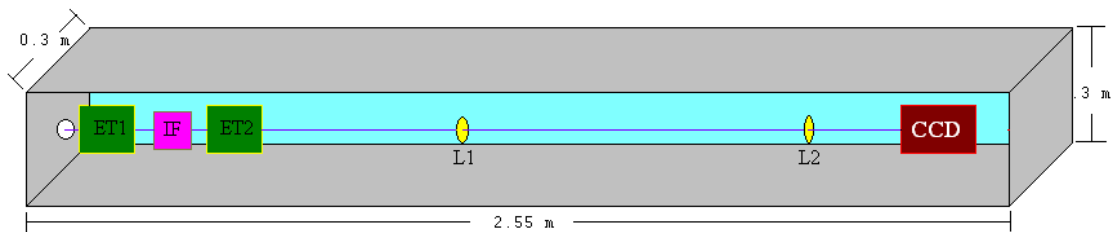


Fig. 8. The approximate dimensions of the enclosure for the imager. ET1 and ET2 are the etalon, and IF is the blocking filter. L1 is the collimator and L2 is the imaging lens.

The working temperature for the etalon and blocking filter will also be fixed at 25°C. Figure 7 shows the dimensions from a preliminary design for the enclosure. The dimensions of the entire enclosure is 2.55m × 0.3m × 0.3m.

5. A note on exposure time and signal to noise ratio

The exposure time is calculated by taking into account the reflectance and transmission of all the optical components placed before the CCD. The exact number of components may vary, but an approximate number is available from the proposed layout of the telescope.

The telescope itself will have 10 mirrors of around 95% reflectivity. The combined transmitted intensity of the beam coming out of the telescope entering into the back-end instrument will be around 60%. The adaptive optics system in the beam will have a few more mirrors and other optical components, and an over all estimate of the total transmitted intensity reaching the narrow band filter is around 40%. The transmission of each of the etalon is around 80% and that of the blocking-filter is around 40%. Assuming a 60% QE for the CCD the overall efficiency of the system will be around 7%. The total number of photons collected by the system per second is given by,

$$N_I = I \cdot \Delta x \cdot \Delta \lambda \cdot \tau \cdot A$$

Where I is the number of photons available near that particular wavelength, Δx is the area imaged, $\Delta \lambda$ the bandwidth, τ the overall efficiency of the system and A the collecting area. The number of photons in the continuum available near 6173Å is around 7.8×10^{18} photons/sec/nm. Δx in the case of our proposed layout is 0.03 arc-sec², the band-width is around 54mÅ and the collecting area of the telescope is 1963cm². Introducing these values in the above equation, the number of photons obtained in the CCD in one second is 4.2×10^6 . This means, to fill 80% (in order avoid any kind of saturation) of the full-well capacity (80 ke⁻) of the CCD (Acton PhotonMAX1024B) it requires 15msec exposure time. The photon noise in the case of a single frame is 252, and the signal-to-noise ratio is around 254. This is true for the measurement in the continuum, but for the magnetic field measurements, normally the images are taken in the wing of the absorption line and this reduces the overall intensity to some extent, i.e. in Fe I 6173Å line the core intensity is only 40% of the continuum. Assuming the filter is tuned to a point where the intensity is around 60% of the continuum, the number of photons available for the *Stokes I* measurement in 15msec is only 2.5×10^4 , which results in a signal to noise ratio of 158. For *Stokes Q*, *U* and *V* parameters, each requires two measurements. For example in *I+V* measurement since $|V| \ll |I|$, we can equate $N_{I+V} \sim N_I$ and the photon noise resulting from this measurement to $\sigma_{I+V} = \sqrt{N_I}$. The uncertainties in *V* and also in *Q* and *U* must be evaluated from error propagation rules, since *V* is computed as $\frac{1}{2}(I+V) - \frac{1}{2}(I-V)$. This gives the square of the uncertainty in *V* as,

$$\sigma_V^2 = \frac{1}{4}\sigma_{I+V}^2 + \frac{1}{4}\sigma_{I-V}^2 \approx \frac{1}{2}N_I$$

We can express the maximum V signal as $\max(|V|) = \varepsilon_v I$, where ε_v is the parameter for the expected signal in terms of I . So the peak signal-to-noise ratio for V can be written as,

$$\frac{V}{\sigma_v} = \frac{\varepsilon_v N_I}{\sqrt{N_I/2}} \approx \varepsilon_v \sqrt{2N_I}$$

For 5G field the expected signal in V is 1.5×10^{-3} . For detecting this signal in V with 3-sigma accuracy, i.e. $V/\sigma_v = 3$, we should have 2×10^6 photons, which could be achieved with 80 frames of 15msec exposures in $I+V$ and $I-V$. Similar measurement in Q and U will provide an accuracy of around 100 G in the transverse field.

Specific measurement steps and data analysis methods for magnetic and Doppler observations will be discussed in a separate technical report.

6. Imager: Development strategy

Major time in the development process will be taken in acquiring various components of the instrument for e.g. minimum time we foresee for acquiring the Fabry-Perot and camera is one year. Our strategy is to develop parallelly all the auxiliary components which we require to run the instrument. Fabrication of some of the major items which will be taken-up while acquiring the optical components are listed below.

- Fabry-Perot etalon and the blocking interference filters require constant temperature ovens. With our present experience, we will be able to design these ovens in-house with appropriate stability. The inputs which we need to know for designing these ovens are the temperature response and the mechanical dimensions of these filters. Blocking interference filters can be purchased in standard sizes, and the dimensions and temperature stability could easily be obtained from the vendor before hand. The temperature response of the Lithium niobate etalon is also well known and this value could be used for deciding the temperature stability of the oven. A dummy holder which will have the same physical dimensions of the real etalon will be asked from the vendor soon after the ordering of the etalons.
- Lithium niobate Fabry-Perot etalons need high voltage power supply for spectral tuning. The development and testing of high-voltage power supply units required for this will be taken-up during the above period. Recently we have developed and tested a 16-bits D/A computer controller for a modular high voltage power supply unit for a similar use.
- Other auxiliary components such as blocking filter wheel (which can incorporate two or more blocking filters), instrument enclosure and other fixtures will also be designed and fabricated during this time period.

By adopting the above strategy, we hope to get the instrument designed, fabricated and tested before the installation of the telescope (which is expected in March 2009).

7. Budget

The major part of the cost involved in developing the narrow band imager will be for acquiring the Fabry-Perot etalons and CCD camera. In table 3 we list the anticipated cost involved in building the imager. The prices are approximate, as available while writing this report.

Table 3. *Anticipated cost involved in developing the narrow-band imger*

Component	Cost
Lithium Niobate Fabry-Perot etalon (CSIRO) ($\times 2$, finesse 25, in simple mounting cell)	$60,00000 \times 2 = \text{Rs. } 120.0 \text{ lakhs}$
Interference blocking filters (centred at 6173\AA and 8542\AA , FWHM = 3\AA and cavities = 2, Andover Corp.)	$1,25000 \times 2 = \text{Rs. } 2.5 \text{ lakhs}$
High voltage power supply modules for etalons ($\times 2$, Applied Kilovolts, $\pm 5\text{kV}$)	$80000 \times 2 = \text{Rs. } 1.6 \text{ lakhs}$
Windows for temperature controlled ovens ($\times 10$, Newport, 50 mm, $\lambda/20$)	$20000 \times 10 = \text{Rs. } 2.0 \text{ lakhs}$
Accessories for high voltage power supply and temperature controller (sensors, D/A converters etc.)	Rs. 75000/-
CCD camera (ActonPhotonMax1024B, back-illuminated)	Rs. 30.0 lakhs
Lenses and other optical elements, opto-mechanical mounts	Rs. 2.5 lakhs
Platform and temperature controlled enclosure	Rs. 1.0 lakh
Total	Rs. 160.35 Lakhs

8. Time schedule

The time required for acquiring the major components such as Fabry-Perot etalons and CCD camera is presumed to be one year. Taking this into account, as discussed in the development strategy, the hardware components required for the imager will be developed during this time. The imager will be made ready by the beginning of 2009, so that it could be used as a first-light instrument. Table 4 give the time schedule for the imager development.

Table 4. *Time schedule for the development*

Internal and external reviews of the proposal	July 20, 2007 – Aug 31, 2007
Revision and modification of the proposal	Sep 01, 2007 – Sep 15, 2007
Floating indents and procurement of components	Sep 16, 2007 – Sep 15, 2008

Development of hardware, developing the optical test setup	Sep 16, 2007 – Sep 15, 2008
Characterisation of Fabry-Perot etalons, filters and assembling the components	Sep 15, 2008 – Feb 15, 2009
Final Narrow band imager in the observing room	March 15, 2009

References :

- [1] *Electro-optic Fabry-Perot Filter: Development for the Study of Solar Oscillations*, C. H. Burton, A. J. Leistner, D. M. Rust, 1987, Applied Optics, **26**, 2637
- [2] *Fabry-Perot filter based Solar video magnetograph*, S. K. Mathew, A. Bhatnagar, C. D. Prasad, & A. Ambastha, 1998, A&AS, **133**, 285
- [3] *TESOS, a double Fabry-Perot instrument for solar spectroscopy*, T. J. Kentischer, W. Schmidt, M. Sigwarth, & M. v. Uexküll, 1998, A&A, **340**, 569
- [4] *Progress report on the Preliminary Design of Multiple Etalon System for the advanced Technology Solar telescope*, G. Allen Gray, K. S. Balasubramaniam, & Brian Robinson, ATST technical report
- [5] *Design and Status of Solar Vector Magnetograph (SVM-I) at Udaipur Solar Observatory*, S. Gosain, P. Venkatakrishnan, K. Venugopalan, 2006, JApA, **27**, 285
- [6] *The Flare Genesis Experiment*, D. M. Rust, G. A. Murphy, K. Strohhahn, S. L. Keil, C. U. Keller, 1996, AAS, **188**, 6705
- [7] *The imaging magnetograph eXperiment for the SUNRISE balloon Antarctica project*, V. Martinez Pillet et al., 2004, SPIE, **5487**, 1152
- [8] *Tunable Narrow-Band Filter for Imaging Polarimetry*, A. Feller, A. Boller, J. O. Stenflo, 2006, ASPC, **358**, 155
- [9] *Magnetic field vector retrieval with the Helioseismic and Magnetic Imager*, J. M. Borrero et al., 2006, Sol. Physics., **240**, 177
- [10] *Experimentally determined r_{13} electro-optic coefficient for a Lithium niobate crystal*, S. K. Mathew, 2003, Applied Optics, **42**, 3580